Soft Matter

Cite this: *Soft Matter*, 2012, **8**, 6731

www.rsc.org/softmatter

PAPER

PFG-NMR self-diffusion measurements in the single phase channels of a microemulsion system with an anionic–nonionic surfactant mixture†

Lukas Wolf,*[a] Heinz Hoffmann,[a] Jürgen Linders[b] and Christian Mayer[b]

Received 3rd December 2011, Accepted 15th April 2012
DOI: 10.1039/c2sm07301c

The single phase channels of a presently reported microemulsion system were investigated by electrical conductivity and pulsed-field gradient nuclear magnetic resonance (PFG-NMR) spectroscopy. The system consists of a mixed anionic–non-ionic surfactant mixture, water and decane. At constant surfactant concentration and temperature, the phase diagram exhibits two single phase microemulsion channels, separated by an anisotropic lamellar channel. The lower microemulsion channel starts from the water side of the phase diagram with a micellar L_1 phase and reaches the middle of the phase diagram with increasing mass fraction of decane in the solvent mixture and increasing mass fraction of lipophilic co-surfactant in the surfactant mixture. The upper microemulsion channel passes from the aqueous side with an L_3 phase to the oil side of the diagram. Conductivity data and self-diffusion coefficients, obtained by PFG-NMR, support the previously made conclusion that the nanostructure in the upper channel undergoes an abrupt transition from a bicontinuous structure to a water-in-oil High Internal Phase Microemulsion (HIPME) with already less than 10% of oil in the solvent mixture, while the structures in the lower microemulsion channel are oil-in-water droplets. The HIPME structure is a feature of the surfactant mixture and probably formed due to a high interfacial tension between the aqueous diluted surfactant phase and the oil. By the addition of salt, the HIPME structures are obviously disturbed, resulting in an increased conductivity and self-diffusion rate for the water fraction.

Introduction

Since their discovery in 1943 by Hoar and Schulman, microemulsions were much in the focus of interest by scientists in the field of colloid and polymer science.[1] They defined microemulsions as optically isotropic transparent phases, consisting of oil, water and surfactants.[2] In contrast to ordinary emulsions, microemulsions are thermodynamically stable.[3] Three different types of nanostructures can be distinguished in microemulsions, namely oil droplets in a continuous water phase (o/w), water droplets in a continuous oil phase (w/o) and bicontinuous structures.[4] The type of the used surfactant plays an important role in the emerging nanostructures. The most detailed investigated microemulsion systems are those with a single non-ionic surfactant C_iE_j, water and oil. In such systems, it is possible to pass from water-rich to oil-rich single phase microemulsions, without crossing a phase boundary in the phase diagram.[5] In order to stay in the single phase region, one has to adapt the hydrophilic lipophilic balance (HLB) by changing the temperature, as non-ionic surfactants are very temperature sensitive.[6] The behaviour and the nanostructures in these single-phase channels are known and theoretically well understood.[7] They have been investigated indirectly by electrical conductivity, small angle neutron scattering (SANS), NMR and directly imaged by freeze fracture transmission electron microscopy (FF-TEM).[8–10] With increasing temperature and increasing oil content but constant surfactant concentration, the structure undergoes a continuous transition from small oil droplets in water at the aqueous side to a bicontinuous structure at the middle of the phase diagram with equal amounts of oil and water to small water droplets in oil at the oil side.[11] The structural transition is caused by the change of the amphiphilic properties of the non-ionic surfactant with rising temperature. Thus, the curvature of the amphiphilic monolayer changes from convex, to flat, to concave.

The situation is somewhat different in microemulsions prepared with ionic surfactants. In such systems, it is not possible to pass from the single aqueous phase to the oil phase without crossing phase boundaries at constant surfactant concentration.[12] The best known systems with ionic surfactants are probably microemulsions with sodium bis(2-ethylhexyl) sulfosuccinate (AOT), decane or di-dodecyl-dimethylammoniumbromide (DDAB), dodecane and water.[13,14] In contrast to

[a] *University of Bayreuth, BZKG/BayKoll, Gottlieb-Keim-Str. 60, D-95448 Bayreuth, Germany. E-mail: lukas.wolf@freenet.de; heinz.hoffmann@uni-bayreuth.de*
[b] *University of Duisburg-Essen, Institute for Physical Chemistry, CeNIDE, D-45141 Essen, Germany. E-mail: juergen.linders@arcor.de; christian.mayer@uni-due.de*

† Electronic supplementary information (ESI) available. See DOI: 10.1039/c2sm07301c

bicontinuous microemulsions with a single nonionic surfactant, in these systems a w/o droplet structure is present at equal amounts of water and oil.[15]

We reported recently a new microemulsion system with a mixed anionic–nonionic surfactant mixture.[16] In such systems it is possible to pass from the aqueous to the oil side in a single phase microemulsion channel at constant surfactant concentration and constant temperature. This is achieved by changing the HLB not by temperature but by adjusting the surfactant–co-surfactant ratio. Conductivity data, electric birefringence measurements and cryo-TEM pictures indicated that the nanostructure in this single phase channel has a w/o-structure at a water–oil ratio of 1/1 and not a bicontinuous structure as achieved with a single non-ionic surfactant. We called this structure High Internal Phase Microemulsion (HIPME). Furthermore, the transition from a bicontinuous L_3 phase to a w/o high internal phase microemulsion seemed to be already completed by solubilising less than 10% oil into the system.[17–19] In this investigation, we want to prove by pulsed-field gradient nuclear magnetic resonance (PFG-NMR) that this is indeed the case. Moreover we investigated the influence of the addition of excess salt to the microemulsion system by interfacial tension measurements, conductivity and PFG-NMR, as it was tried to transform the HIPME structures to bicontinuous structures by shielding the charge of the anionic surfactant.

Results and discussion

Surface and interfacial tension measurements

The binary surfactant mixture of our reported microemulsion system is composed of the hydrophilic anionic surfactant Magnesium Dodecyl Sulfate $Mg(DS)_2$ and the lipophilic non-ionic co-surfactant iso-tridecyl-triethyleneglycolether IT 3 ($C_{13}E_3$). We chose the Mg-salt of SDS, as it is known to cause lower surface tension values than SDS and it is possible to form sponge like L_3 phases with co-surfactants.[20,21] The surface tension and the interfacial tension between the aqueous surfactant and the oil phase play an important role in the formation of microemulsions with non-ionic surfactants.[22] Optimal solubilisation of oil should occur when the interfacial tension of the dilute surfactant solution is the lowest against the oil phase.[23] Low interfacial tension values are observed for surfactant systems which form liquid crystalline L_α or L_3 phases at low surfactant concentrations.[24] The surfactant mixture at a mixing ratio of 1/1 (w/w) of both surfactants has a critical micelle concentration (cmc) at a value around 0.025% surfactant and reaches a very low surface tension of ~26 mN m^{-1}. This is indeed a very low value, if one considers the surface tension of SDS around 35 mN m^{-1} above its cmc.

The interfacial tension of diluted surfactant mixtures against the oil decane runs through a broad minimum with increasing mass fraction of the co-surfactant IT 3 in the surfactant mixture. The minimum of the interfacial tension is reached between the mass fraction x IT 3 = 0.4 and 0.5 with a value of ~2.3 mN m^{-1}. In this area, the binary surfactant mixture starts forming single phase liquid crystalline L_α phases at higher surfactant concentrations.[18] The data are very similar compared to a previously investigated microemulsion system with a silicone oil.[16] In contrast to microemulsions with a single non-ionic surfactant, where ultra-low interfacial tensions in the range of 10^{-3} mN m^{-1} are reached, the values with our surfactant system are surprisingly high and theoretically too large for the formation of microemulsions by taking into account typical calculation models. However, the interfacial tension of double chain surfactants, which have been used for the preparation of microemulsions, against oil is also high and in a similar range of 0.1–1 mN m^{-1}.[31] One possible reason for the high interfacial tension values might be the charge of the anionic surfactant. In systems with ionic surfactants, it is often possible to lower the interfacial tension by shielding the electric charge with excess salt.[32] Detailed curves for the measured surface and interfacial tensions are shown in the ESI (SI1 and 2†).

Phase diagram of $Mg(DS)_2$/IT 3–H_2O/*n*-decane

A phase diagram of our investigated microemulsion system is shown in Fig. 1. The total surfactant concentration was kept constant at 15% (w/w) and the temperature at 25 °C. Samples were prepared with 20% glycerine in H_2O to prevent freezing artefacts in freeze fracture transmission electron microscopy (FF-TEM) investigations that were done previously.[18] The phase diagram contains two isotropic microemulsion channels, a lower one and an upper one. The upper one begins on the surfactant axis at the region of the L_3 phase. With increasing oil, the channel first shifts to a lower IT 3 ratio and then again to a higher IT 3/$Mg(DS)_2$ ratio for higher oil ratios. It ends on the oil side at 80% decane and pure IT 3 as the surfactant. The lower channel begins at the L_1 region and ends in the middle of the phase diagram at an IT 3 ratio of 0.57. Both channels are separated by a large single phase birefringent L_α region that extends from 0% to 90% decane with slightly increasing mass fraction of IT 3.

The microemulsions in the lower single phase channel are transparent phases that show no flow birefringence under shear. The samples in the upper phase channel have different properties. While the L_3 phase without decane is completely transparent, the

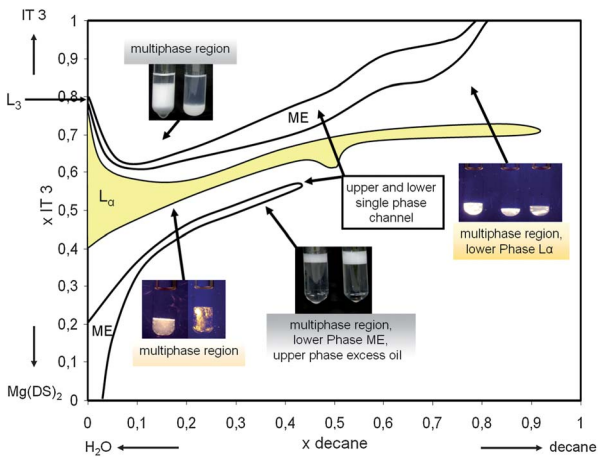

Fig. 1 Phase diagram of the system $Mg(DS)_2$/IT 3–H_2O/decane at 15% (w/w) surfactant and 25 °C, 20% glycerin in H_2O. x IT 3 = mass fraction of IT 3 in the surfactant mixture, x decane = mass fraction of decane in the solvent mixture. "ME" indicates isotropic microemulsion area, L_α indicates the area of the anisotropic lamellar channel.

samples with decane look somewhat bluish and their scattering intensity is most intensive around x decane 0.03 to 0.1. For higher oil content the scattering intensity decreases again.

A good and quick method that gives first indications for the nanostructures in microemulsions is the measuring of the electric conductivity. It helps to distinguish between conducting water continuous phases and non-conducting oil continuous phases.[26] Because we use a surfactant mixture with an anionic surfactant, no additional salt has to be added to follow the conductivity in the phases in contrast to microemulsions with only a single non-ionic surfactant. The plots of the conductivities in the upper and lower single phase channels are shown in Fig. 2a and b. In the upper channel, the conductivity first increases slightly from around 1000 μS cm^{-1} of the sample without decane to 1160 μS cm^{-1} to the sample with 1% decane. The reason for this lies in the change of the composition of the surfactant mixture. In the range from 1% to 10% decane, the conductivity decreases abruptly three orders of magnitude to 1 μS cm^{-1} even though the fraction of the anionic $Mg(DS)_2$ is increasing. For higher mass fractions of decane, the conductivity values decrease continuously to low values as *e.g.* 0.03 μS cm^{-1} for the sample with a water–oil ratio of 1/1 (w/w). The conductivities thus indicate a dramatic change in the nanostructure of the upper channel with solubilisation of small amounts of oil into the L_3 phase. The abrupt collapse of the conductivity indicates that the system changes from a bicontinuous structure to a water-in-oil (w/o) structure. Conductivities in the isotropic channels of microemulsions from non-ionic surfactants have been reported in the literature.[27] In such systems, the conductivity in the upper channel decreases continuously with increasing oil content. These measurements have helped to establish the view which we have today from the structures in the upper channel.

It is assumed that with increasing oil content the bicontinuous L_3 phase swells with the solubilised oil between the bilayers and is finally transformed at high oil content to a w/o system. With equal amount of oil and water, SANS-data and conductivities show that this phase is still a bicontinuous phase.[28] Our conductivity data unambiguously show that the structures in the upper channel of the presently investigated system are different from the structures of known systems with non-ionic surfactants. We find a rather abrupt transition from the bicontinuous L_3 structure to a w/o structure with only 10% of oil in the solvent mixture. Recently published cryo-TEM pictures show a polyhedral w/o foam structure, when 6% of oil was solubilised in the L_3 phase.[19] These structures were similar to those that are found in so-called High Internal Phase Emulsions (HIPE).[29] We therefore called the new microemulsion structures High Internal Phase Microemulsions (HIPMEs).

In opposition to the upper channel, the conductivity data of the lower channel indicate that the nanostructure in the lower channel does not change much with increasing oil content. At the water corner, the conductivity in the lower channel with 2900 μS cm^{-1} is much higher than the conductivity of the L_3 phase of the upper channel with 1000 μS cm^{-1}. The reason for this is that the $Mg(DS)_2$ concentration is much higher in the lower channel. With increasing oil content, the conductivities decrease slightly to 1500 μS cm^{-1} at the middle of the phase diagram, which is where the channel ends. The reason for the decrease is mainly the decreasing mass fraction of $Mg(DS)_2$. Obviously, the lower channel consists of a continuous water phase in which oil droplets are dispersed (o/w-structure).

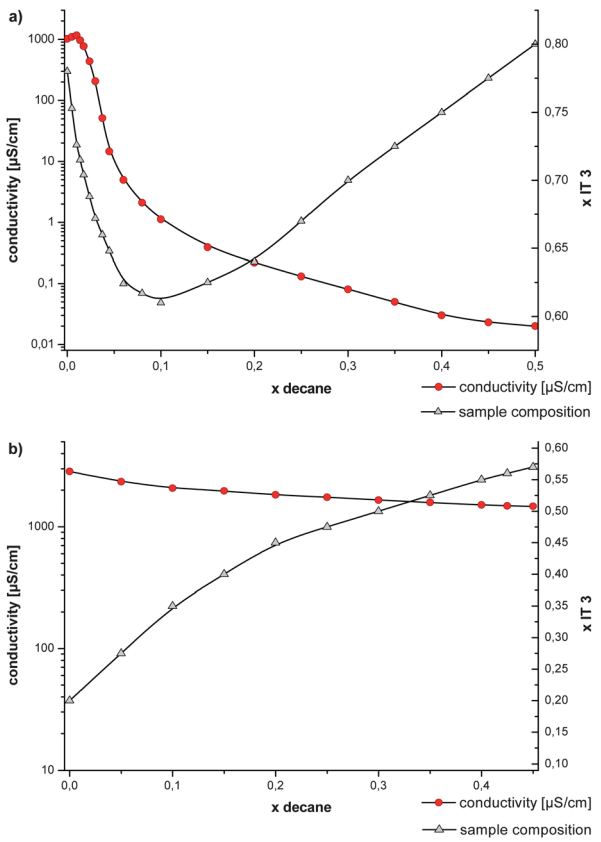

Fig. 2 Plot of conductivity (red dots) and IT 3 content (grey triangles) against the mass fraction of decane in the solvent mixture. (a) Conductivity data for the upper single phase channel. (b) Conductivity data for the lower single phase channel.

PFG-NMR in the microemulsion channels

To underline and to verify our results, we investigated the microemulsion channels by PFG-NMR, as this method delivers information about the structure, fluidity and emulsion type.[33–35] Furthermore, it can give indications about the interaction between the surfactant and co-surfactant at the interface. Fig. 3 shows a conventional proton NMR spectrum of the system in the upper channel at x decane 0.7 and x IT 3 0.85.

The PFG-NMR analysis is focussed on those spectral regions which can either be clearly assigned to single system constituents (water between 4.8 and 5.3 ppm and decane between 1.3 and 2.0 ppm) or to the mixture of the surfactants ($Mg(DS)_2$/IT 3 between 0.2 and 0.4 ppm). The integrals of these three spectral regions strongly depend on the strength of the gradient pulse, thereby indicating the average displacement of the corresponding system constituents during the period between the pulses which was set to 50 ms. For free self-diffusion, the relative echo signal I/I_0 follows the function

$$I/I_0 = \exp[-\gamma^2 G^2 \delta^2 D(\Delta - \delta/3)] \quad (1)$$

with γ being the gyromagnetic ratio of protons, G the strength of the gradient field, D the self-diffusion coefficient, δ and Δ the

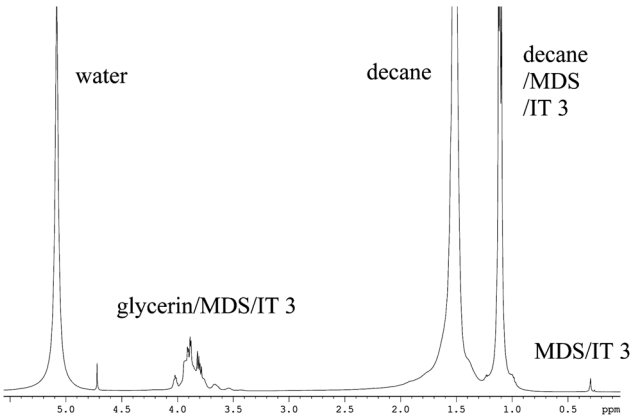

Fig. 3 Proton NMR spectrum of the system in the upper channel at *x* decane 0.7 and *x* IT 3 0.85.

duration of and the spacing between the two gradient pulses. Hence, in a plot of the logarithmic relative signal intensity ln I/I_0 *vs.* the parameter $\gamma^2G^2\delta^2(\Delta - \delta/3)$ the slope is equal to the negative self-diffusion coefficient D of the given component (Stejskal–Tanner plot). If the observed component is located in two different environments leading to clearly different self-diffusion properties, the plot will show two sections with clearly different slopes. If the component is encapsulated in very small droplets, the motion within the droplets becomes undetectable. In this case, the observed slope reflects the diffusive dislocation connected to the Brownian motion of the droplets. For comparison, we introduce reference values for the self-diffusion coefficients of water in aqueous glycerol solution (20%): $D_w^0 = 1.35 \times 10^{-9}$ m^2 s^{-1}, of glycerol in aqueous glycerol solution (20%): $D_g^0 = 4.09 \times 10^{-10}$ m^2 s^{-1}, of $Mg(DS)_2$ in aqueous $Mg(DS)_2$ solution (7.5%): $D_M^0 = 7.21 \times 10^{-12}$ m^2 s^{-1}, of IT 3 in aqueous IT 3 solution (7.5%): $D_{IT\,3}^0 = 6.24 \times 10^{-11}$ m^2 s^{-1} and of decane in pure decane: $D_d^0 = 1.24 \times 10^{-9}$ m^2 s^{-1}.

The resulting Stejskal–Tanner plots for four different states in the upper channel are shown in Fig. 4. The corresponding apparent self-diffusion coefficients, obtained by fitting the data using eqn (1), are listed in Table 1. Examples for the fits are shown in the ESI†. The first plot (Fig. 4a) reflects the situation in the absence of decane (*x* decane 0). Here, the water signal follows a steep decay, corresponding to a self-diffusion constant of $D_w = 6.80 \times 10^{-10}$ m^2 s^{-1}. This is somewhat lower than the reference value for water D_w^0, indicating that water, forming a continuous phase, is slightly affected by dispersed phase boundaries. In contrast, the signal for $Mg(DS)_2$/IT 3 follows a relatively flat decay, pointing to a structure of the surfactant which only allows a restricted mobility of $Mg(DS)_2$ and IT 3 molecules.

The situation changes significantly on the addition of 10% decane (*x* decane 0.1, Fig. 4b). Now the mobility of water is reduced by a factor of three to $D_w = 2.22 \times 10^{-10}$ m^2 s^{-1}. All other system constituents, decane as well as the surfactants, exhibit curved decay profiles indicating two distinctly different self-diffusion constants for each constituent. The largest portion of decane (and a small portion of the surfactants) shows a self-diffusion constant which, with $D_d = 3.65 \times 10^{-10}$ m^2 s^{-1}, is only slightly less than one third of the value for bulk decane.

With the relatively small decane content, this indicates that we actually deal with a continuous decane phase strongly hindered

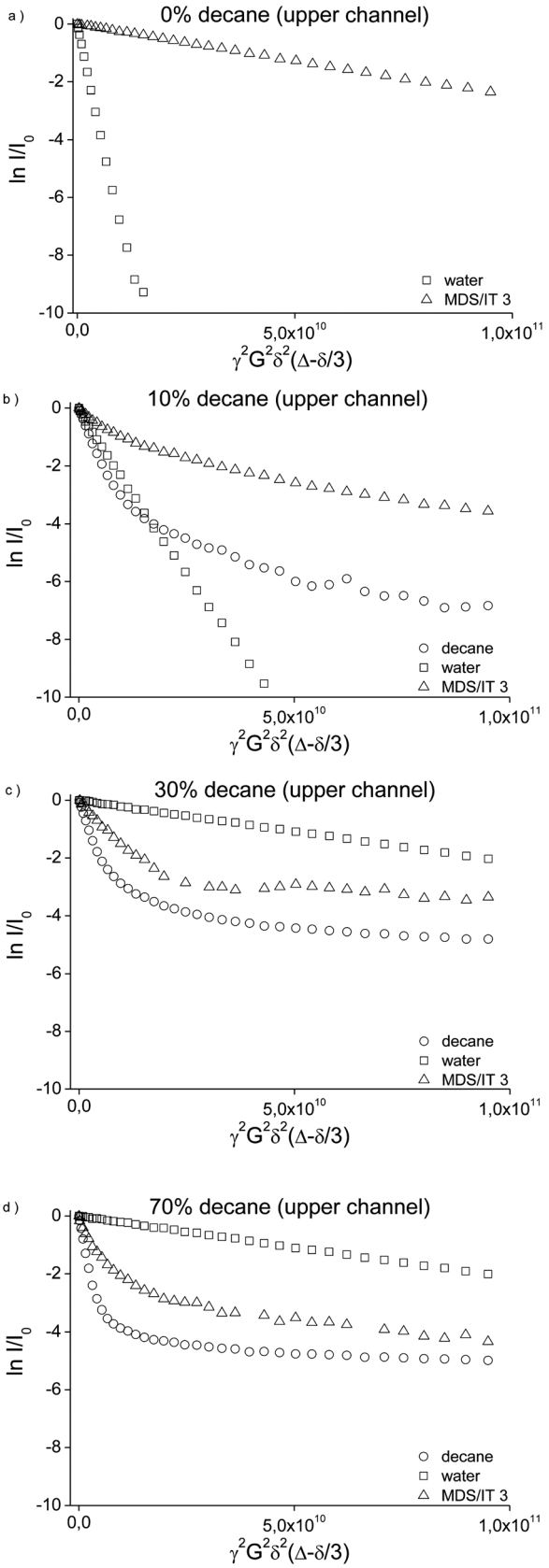

Fig. 4 (a–d) Stejskal–Tanner plots for decane, water and the surfactants in the upper channel.

Table 1 Apparent self-diffusion coefficients of system constituents in the upper channel

x water	*x* decane	*D* (water) [$m^2 s^{-1}$]	*D* (decane) [$m^2 s^{-1}$]	*D* (decane) plateau [$m^2 s^{-1}$]
1	0	6.80×10^{-10}	—	—
0.9	0.1	2.22×10^{-10}	3.65×10^{-10}	5.68×10^{-11}
0.7	0.3	2.14×10^{-11}	4.32×10^{-10}	1.02×10^{-11}
0.5	0.5	9.41×10^{-12}	6.48×10^{-10}	5.74×10^{-12}
0.3	0.7	2.13×10^{-11}	7.07×10^{-10}	8.76×10^{-12}

by dispersed phase boundaries. At the same time, the conductivity data clearly indicate that the aqueous phase is non-continuous. The slower portion of the decane (approximately 3%) seems to be associated with the majority of the surfactant ($D_d = 5.68 \times 10^{-11}$ m^2 s^{-1}).

Altogether, the self-diffusion profile is compatible with a high internal phase w/o-microemulsion (w/o-HIPME) of 90% water in 10% decane. Obviously, a small fraction of the decane is closely associated with the surfactant layer which explains the slow fraction of decane. Correspondingly, some of the surfactant is being dissolved in the decane phase which explains the fast fraction of the $Mg(DS)_2$/IT 3 signal. The high self-diffusion rate of the water indicates significant exchange of water molecules *via* the thin decane films which separate the water droplets.

With increasing decane content (*x* decane 0.3, 0.5 and 0.7), the system gradually changes towards a conventional water in oil microemulsion (Fig. 4c and d, Table 1). The mobility of water is further reduced by an order of magnitude to $D_w = 2.14 \times 10^{-11}$ m^2 s^{-1} and $D_w = 2.13 \times 10^{-11}$ m^2 s^{-1}, respectively. In addition, the mobility of the surfactant as well as the "slow" fraction of the decane is slowed down by a factor of five ($D_d = 1.02 \times 10^{-11}$ m^2 s^{-1}, $D_d = 5.74 \times 10^{-12}$ m^2 s^{-1} and $D_d = 8.76 \times 10^{-12}$ m^2 s^{-1} for *x* decane 0.3, 0.5 and 0.7). In contrast, the "fast" fraction of the decane exhibits values which now come close to the bulk self-diffusion rate of $D_d^0 = 1.24 \times 10^{-9}$ m^2 s^{-1} ($D_d = 4.32 \times 10^{-10}$ m^2 s^{-1}, $D_d = 6.48 \times 10^{-10}$ m^2 s^{-1} and $D_d = 7.07 \times 10^{-10}$ m^2 s^{-1} for *x* decane 0.3, 0.5 and 0.7). In this situation, the observed dislocation for water molecules is largely caused by the Brownian motion of small water droplets in the continuous decane phase. With the given viscosity of decane at room temperature, the diameter of the water droplets can be estimated to be approximately 20 nm. As before, we assume that part of the surfactant is dissolved in the continuous decane phase, leading to the initial fast decay of the $Mg(DS)_2$/IT 3 signal. Also, again a small fraction of the decane is dissolved in the surfactant layer around the water droplets, leading to the shallow plateau of the decane signal. The fact that the self-diffusion coefficient for water is still slightly larger than for the droplet wall constituents indicates the exchange of a small fraction of water molecules between the droplets *via* the hydrophobic phase, an effect which is linked to Ostwald ripening.

In contrast to the results for the upper channel, the variations between the PFG-NMR results of different positions in the lower channel do not indicate dramatic structural changes, even though self-diffusion constants do vary significantly with *x* decane. An example for a corresponding Stejskal–Tanner plot for the lower channel is shown in Fig. 5. Apparent self-diffusion coefficients for two points in the lower channel are listed in Table 2. The data for water and the surfactants resemble those of the upper channel in the absence of decane. Again, the water signal shows very steep decays linked to self-diffusion coefficients of 1.04×10^{-9} m^2 s^{-1} for *x* decane 0.1 and 8.36×10^{-10} m^2 s^{-1} for x decane 0.3, values which come close to the water reference ($D_w^0 = 1.35 \times 10^{-9}$ m^2 s^{-1}). In contrast, the decane signal indicates an increasingly slow mobility (1.37×10^{-11} m^2 s^{-1} and 2.88×10^{-13} m^2 s^{-1}) which corresponds to the Brownian motion of droplets with increasing size. The very large difference between the two self-diffusion constants of decane may at least in parts be explained by the obstruction effect[36] expected for the given high volume fractions of dispersed droplets in the case of *x* decane = 0.3. The surfactant seems to be linked to the decane droplets, even though the self-diffusion rate is slightly larger. The latter indicates some monomeric solubility of the surfactant in the aqueous phase. All in all, the data are clearly in accordance with an o/w microemulsion with the droplet size significantly growing with the decane content. Parts of the surfactant molecules may undergo more rapid self-diffusion *via* molecular exchange with micelles which would explain for the slight deviation between the slopes for the decane and the surfactant signals. An extremely small fraction of water molecules may be linked to the droplets and explain a possible plateau of the water signal for $\ln I/I_0 < -8$. However, with a contribution of only 0.01%, this signal fraction comes close to the noise amplitude and may be insignificant. For a better overview, the self-diffusion constants *D* for H_2O and decane are summarized in Fig. 6 as a function of the decane content.

The data for the water fraction show a clear correlation with the corresponding conductivity plots in Fig. 2. In the upper channel, the water mobility steeply declines with increasing decane concentration (Fig. 6). This behavior is reproduced by a corresponding decrease of the conductivity (Fig. 2a) which can be regarded as a direct consequence: with less mobile water molecules, ions in the aqueous solution can be expected to be less mobile as well. However, this effect is far more dramatic on conductivity than on the mobility of individual water molecules: a reduction of the self-diffusion coefficient by a factor of 30 results in a loss in conductivity by more than three orders of magnitude. This may be partially explained by a reduced overall ion concentration connected to the decreasing water content.

In the case of the lower channel, the loss of water mobility under increasing decane content is much smaller (Table 2). This

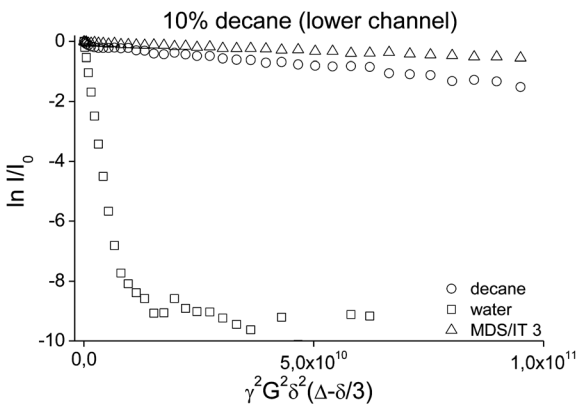

Fig. 5 Stejskal–Tanner plots for decane, water and the surfactants in the lower channel.

Table 2 Apparent self-diffusion coefficients of system constituents in the lower channel

x water	*x* decane	*D* (water) [m^2 s^{-1}]	*D* (water) plateau [m^2 s^{-1}]	*D* (decane) [m^2 s^{-1}]
0.9	0.1	1.04×10^{-9}	1.79×10^{-11}	1.37×10^{-11}
0.7	0.3	8.36×10^{-10}	9.04×10^{-12}	2.88×10^{-13}

is again reflected by the conductivity data (Fig. 2b) which show a minor decrease on addition of decane. Here, a decrease of the water mobility by a factor of 1.2 between *x* decane 0.1 and 0.3 is accompanied by about the same factor of 1.25 in conductivity. The reason for this lies mainly in the decreasing mass fraction of the anionic $Mg(DS)_2$ in the surfactant mixture.

Influence of salt on the system

As already mentioned, our mixed anionic–nonionic surfactant system has a very high interfacial tension against the oil phase compared to the ultra-low interfacial tensions that can be reached with single non-ionic surfactants. We assumed that shielding the charge of the anionic surfactant by adding excess salt would lower the interfacial tension.

Similar effects were already reported for the anionic surfactant diethylhexyl sodium sulfosuccinate (AOT), where ultra-low interfacial tensions against oil were reached with additional NaCl.[25]

To verify our assumption, we measured the interfacial tension at two mixing ratios of the surfactant and co-surfactant with increasing amount of NaCl, namely around the minimum of the observed interfacial tension at *x* IT 3 = 0.5 and around the mixing ratio of the L_3 phase at *x* IT 3 = 0.8. However, the interfacial tension was lowered only about 0.5 mN m^{-1} at the minimum of the interfacial tension at *x* IT 3 = 0.5 and only about 0.9 mN m^{-1} around the L_3 phase at *x* IT 3 = 0.8, when the molar ratio of $Mg(DS)_2$: NaCl in the surfactant mixtures is raised to 1 : 1. No ultra-low interfacial tensions were detected. Detailed results are shown in the ESI (SI3†). We also checked the influence of salt on the phase behaviour of the upper microemulsion channel. Therefore, we had a closer look at the microemulsion with 30% decane in the solvent mixture and investigated how the phase boundaries would shift by adding NaCl to the system. It turned out that the upper and lower borders of the single phase region are shifted to lower *x* IT 3 values by *x* IT 3 ≈ 0.07 when we added NaCl to the $Mg(DS)_2$ in a molar ratio of 1 : 1. The shift to lower *x* IT 3 values means that the system in total becomes more lipophilic, as less amount of the lipophilic co-surfactant IT 3 in the surfactant mixture is needed to solubilise 30% of decane. The shift of the phase boundaries accompanied also by a change in the nanostructure was first investigated by measuring the electric conductivity of the microemulsion with increasing salt concentration. A plot of the conductivity in the single phase region with increasing NaCl concentration is shown in Fig. 7.

The conductivity from the NaCl-free microemulsion to the microemulsion with a molar ratio of $Mg(DS)_2$: NaCl = 1 : 1 increases about three orders of magnitude from a low value of 3 μS cm^{-1} to ~1000 μS cm^{-1}. The conductivity increases in a sigmoid curve with an inflection point around 50% NaCl and not linearly with increasing NaCl concentration. At first sight, the nanostructure seems to change from a w/o-HIPME system to a bicontinuous-like nanostructure.

To verify this, we compared two microemulsions with different salt concentrations by PFG-NMR. The first sample without NaCl had the composition of *x* IT 3 0.7 and *x* decane 0.3. The second sample had the composition of *x* IT 3 0.615, *x* decane 0.3, and the molar ratio of $Mg(DS)_2$: NaCl = 1 : 1. The resulting Stejskal–Tanner plots are shown in Fig. 8 and the corresponding apparent self-diffusion constants are listed in Table 3.

Obviously, the signal decay plot of decane does not change significantly on the addition of NaCl. Hence, we believe that decane remains in a continuous phase after addition of the salt. The signal decay for H_2O, however, changes drastically. The mobility of the water signal of the sample containing NaCl is increased to $D_w = 9.21 \times 10^{-11}$ m^2 s^{-1}. Nevertheless, it is still about a factor 2 smaller compared to the water signal of the HIPME-sample containing 10% decane without NaCl. It is likely that the water only can diffuse slowly through the organic phase. Although the conductivity results indicate a transition from a HIPME structure to a bicontinuous structure by adding salt to the microemulsion, this is definitely not the case. First of all, one

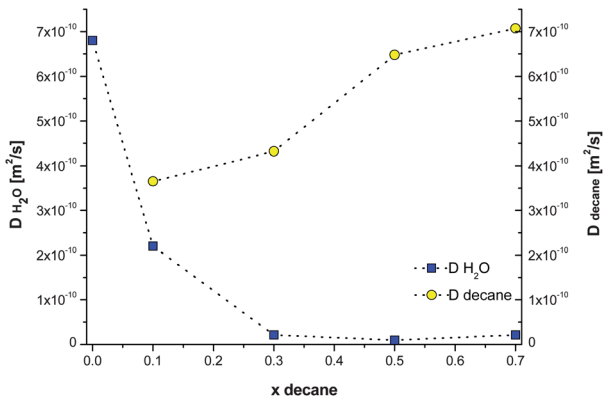

Fig. 6 Overview of self-diffusion coefficients *D* for H_2O and decane in dependency of the decane content in the upper microemulsion channel.

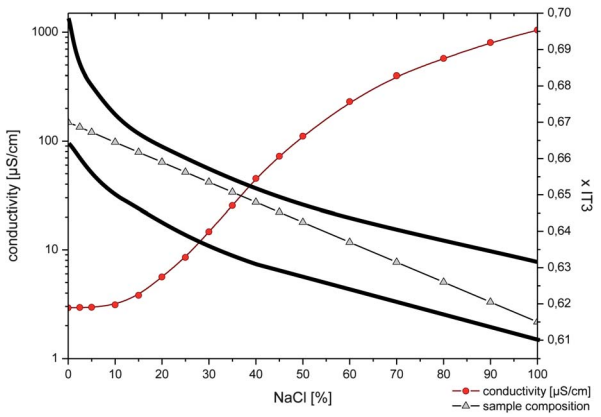

Fig. 7 Plot of conductivity in the single phase region of a microemulsion with *x* decane 0.3 and increasing NaCl concentration at 25 °C. Thick black lines indicate phase boundaries of the single phase region. 100% NaCl corresponds to a molar ratio of $Mg(DS)_2$: NaCl = 1 : 1.

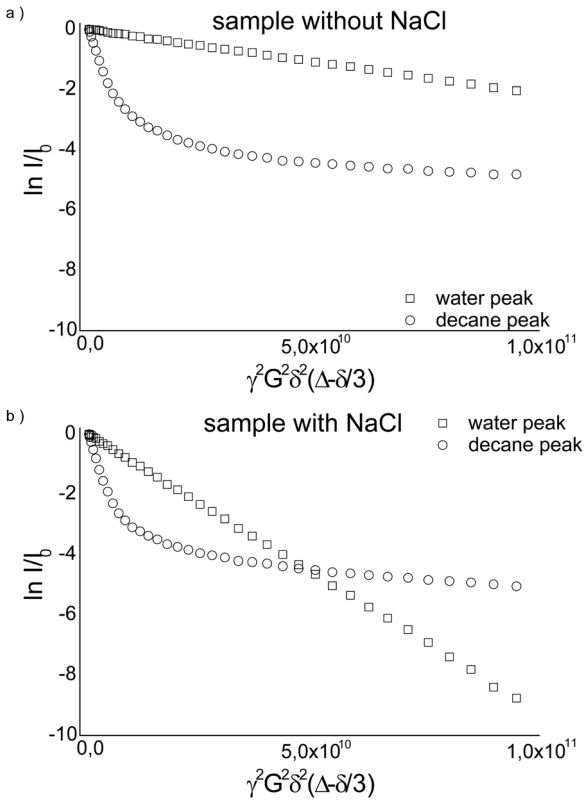

Fig. 8 Stejskal–Tanner plots for decane and water at *x* IT 3 0.7 and *x* decane 0.3 in the absence (top) and presence (bottom) of NaCl.

has to reconsider precisely the conductivity value of the transformed microemulsion with NaCl. This microemulsion has a fraction of ~5.8% $Mg(DS)_2$ (*x* IT 3 = 0.615) in the sample. This corresponds to a molar concentration of ~105 mM $Mg(DS)_2$. The molar ratio of $Mg(DS)_2$: NaCl in this sample was 1 : 1. A 100 mM NaCl standard solution has a conductivity of about 11 mS cm^{-1}. The conductivity value of the microemulsion with NaCl is already about 10 times lower than this value. Secondly, the self-diffusion coefficients for the water fraction of the sample containing NaCl are far away from bulk-water, whereas the decane-signal does not change at all when salt is added to the system. Thus we assume that the morphology cannot be a bicontinuous sponge-like structure as it is the case for microemulsions with a single non-ionic surfactant. It is conceivable that the charge on the surfactant monolayer with the anionic surfactant is shielded by the addition of NaCl and thus the repulsion forces are decreased. Consequently the system becomes highly dynamic. This might allow some water-domains to fuse together and form passages, in which the ions could be transported in the aqueous phase and therefore increase the

Table 3 The influence of electrolyte on the apparent self-diffusion coefficients of system constituents in the upper channel

Sample	*D* (water) [m^2 s^{-1}]	*D* (decane) [m^2 s^{-1}]	*D* (decane) plateau [m^2 s^{-1}]
Without NaCl	2.14×10^{-11}	4.32×10^{-10}	1.02×10^{-11}
With NaCl	9.21×10^{-11}	4.68×10^{-10}	1.72×10^{-11}

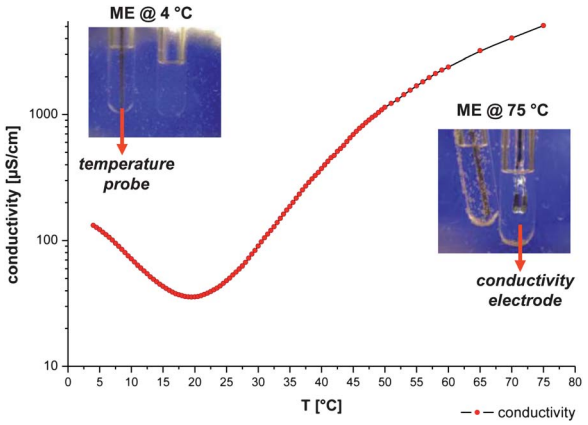

Fig. 9 Conductivity of a microemulsion from the upper single phase channel with increasing temperature. Sample composition: *x* IT 3 0.64, *x* decane 0.3, molar ratio of $Mg(DS)_2$: NaCl = 2 : 1. Phase behaviour of the microemulsion investigated by visual observation between crossed polariser foils.

conductivity of the system. For that reason we assume the nanostructure with NaCl to be more a HIPME-structure with defects in the form of bent water-domains than a classical bicontinuous sponge phase. It is, however, unclear, why there is such a discrepancy between the comparably small self-diffusion constant for the water fraction and the high conductivity value.

Temperature stability of the microemulsions

Another interesting question emerges, namely how the microemulsion reacts to temperature changes. In order to examine this, we chose the microemulsion at the turning point of Fig. 7 for investigations, as we assumed that it might be highly sensitive for conductivity changes with temperature. For this experiment, we raised the temperature of the microemulsion by ~0.5 °C per minute and noted the change of the conductivity. The result is shown in Fig. 9.

The first astonishing result of this experiment was that the microemulsion didn't phase separate in an enormous temperature range from about 4 °C to 80 °C. This was checked by visual observation of the sample between crossed polariser foils. The high temperature stability of the sample is due to the fact that the HLB of the surfactant mixture is more determined by the mixing ratio than by the temperature. Although the non-ionic compound IT 3 becomes more lipophilic by raising the temperature as any other surfactant of the type C_iE_j, the anionic surfactant becomes more hydrophilic, compensating the effect of the non-ionic co-surfactant. This idea was already proposed in the literature.[30] The conductivity runs through a minimum of ~30 µS cm^{-1} around 20 °C and increases to 5000 µS cm^{-1} at 75 °C, indicating various changes in the nanostructure of the microemulsion with increasing temperature.

Conclusion

We have shown by PFG-NMR that the nanostructure in the upper microemulsion channel of a mixed anionic–nonionic surfactant mixture transforms from a bicontinuous L_3 phase to a w/o-HIPME structure with less than 30% of oil in the solvent

mixture, while the lower microemulsion channel has an o/w structure. The results are in good agreement with conductivity data and cryo-TEM pictures that were published recently. Moreover, these microemulsions are highly temperature stable. By addition of NaCl, the conductivity and the mobility of H_2O increase significantly. Nevertheless, it is unlikely that the nanostructures with NaCl have the same sponge-like morphology as bicontinuous microemulsions with single non-ionic surfactants, as the conductivity values are much lower than expected for a real bicontinuous microemulsion and the NMR signals still indicate the presence of a HIPME-structure. Based on NMR and conductivity results, we assume the structure to be a HIPME-phase with defects in relation to the isolated water-domains. The question, how the nanostructure is influenced exactly by the addition of NaCl, can surely be answered by further cryo-TEM or FF-TEM experiments.

Experimental

Materials

The non-ionic surfactant iso-tridecyl-triethyleneglycolether ($C_{13}E_3$), abbreviated as IT 3, was obtained from the Sasol Company (Hamburg, Germany) under the name "Marlipal O13/30". This compound has a polydisperse distribution of EO-groups with an average 3 EO-units. Sodium dodecyl sulfate (SDS, cryst. research grade) was purchased from the Serva Company (Heidelberg, Germany). $MgCl_2 \cdot 6H_2O$ was purchased from the Grüssing Company (Filsum, Germany). *N*-Decane (analytical grade) was obtained from the Merck Company (Darmstadt, Germany).

Preparation of $Mg(DS)_2$

For the preparation of $Mg(DS)_2$, 400 mM SDS-solution was mixed with 200 mM $MgCl_2$ solution under stirring. The bivalent counter ion Mg^{2+} binds stronger to the dodecyl sulfate than the sodium ion, leading to a precipitation of $Mg(DS)_2$ in solution below its Krafft-temperature around 25 °C. The solution was heated up above 25 °C to obtain a clear solution, and then cooled down to 20 °C. After precipitation overnight, $Mg(DS)_2$ was filtered and washed several times with de-ionised water to remove excess salt. The purity of the surfactant thus could be checked by measuring the conductivity of the flow through the filtered $Mg(DS)_2$. The washed $Mg(DS)_2$ was freeze-dried with the freeze-drying device Alpha 1-4, from the Christ Company (Osterode, Germany) and used without further purification.

Preparation of samples

All samples were prepared by weighing directly the components in test tubes on an analytical balance. The test tubes were sealed with Teflon tape, tempered at 25 °C in a water bath, and vortexed several times thoroughly. All samples were incubated at least 3 days at 25 °C before being investigated for their phase behaviour. In general, a phase diagram was scanned with a resolution of 5% in the composition of the mass fraction of IT 3 and decane. Finer steps were investigated in the beginning of the narrow upper single-phase channel. The multiphase samples were viewed and imaged without and in between crossed polarisers to visualise the birefringence of lamellar regions.

Conductivity measurements

For conductivity measurements, Microprocessor Conductivity Meter LF3000 from the WTW Company (Weilheim, Germany) was used. Before measuring, the electrode was tested by checking the conductivity of 10 mM and 100 mM KCl solutions and determining the correct cell constant. Samples were tempered with a RM6 circulating bath from the Lauda Company (Koenigshofen, Germany). The temperature of the measured samples was checked with the GMH 3750 High Precision Digital Thermometer from the Greisinger Company (Regenstauf, Germany). The temperature probe was placed directly into a water filled test tube next to the microemulsion sample. During conductivity measurements, the microemulsion samples were observed between crossed polarisers for their phase behaviour.

Surface/interfacial tension measurements

The surface and interfacial tensions were measured with the volume-drop tensiometer TVT1 from the Lauda Company (Koenigshofen, Germany). The device was set to standard mode with a constant drop-volume creation speed of 3 s μl^{-1}. To assure that the drop creation speed was not set too fast, time dependent measurements were carried out. For interfacial tension measurements, a surfactant concentration of 0.5% (w/w) for the surfactant mixtures was chosen that was about one order of magnitude higher than the cmc of the surfactant mixture at a ratio of 1/1. The interfacial tension of the diluted surfactant mixtures was measured directly against decane.

Pulsed-field gradient nuclear magnetic resonance spectroscopy (PFG-NMR) self-diffusion measurements

For the preparation of the PFG-NMR samples, a regular 3 mm NMR sample tube was filled and embedded in an outer 5 mm sample tube filled with D_2O (lock). All PFG-NMR-measurements were performed on a Bruker DRX 500 spectrometer (Bruker AG, Karlsruhe, Germany) equipped with a BAFPA 40 gradient amplifier and a Bruker DIFF30 probe. The instrument was tuned to 500 MHz proton frequency and gradient pulses were adjusted to gradient strengths between 5 and 450 gauss per cm with individual durations of 2 ms. For all measurements, the stimulated echo ($90°$–τ_1–$90°$–τ_2–$90°$–τ_1–echo) was used in combination with the gradient pulses during each τ_1 waiting period. The duration of the $90°$ pulses was 8.67 μs, the waiting period between the 32 repetitions (scans) of each experiment amounts to 11 s. The spacing Δ between the two gradient pulses was 50 ms. The free induction decays resulting from the addition of each set of 32 experiments were Fourier transformed and analyzed for the echo signal decay *vs.* the gradient strength G and the pulse spacing Δ. Characteristic signals were chosen for the individual observation of decane, water and MDS/IT 3. For the analysis of the self-diffusion profile, the relative signal intensities I/I_0 (I_0 referring to the signal intensity at the gradient strength $G = 0$) were plotted logarithmically *vs.* the parameter $\gamma^2 G^2 \delta^2 (\Delta - \delta/3)$, with γ being the gyromagnetic ratio of protons, G the

strength of the gradient field, δ and Δ the duration of and the spacing between the two gradient pulses.

Notes and references

1 T. P. Hoar and J. H. Schulman, *Nature*, 1943, **152**, 102–103.
2 J. H. Schulman, W. Stoeckenius and L. M. Price, *J. Phys. Chem.*, 1959, **63**, 1677–1680.
3 M. Gradzielski and H. Hoffmann, *J. Phys. Chem.*, 1994, **98**, 2613–2623.
4 F. Lichterfeld, T. Schmeling and R. Strey, *J. Phys. Chem.*, 1986, **90**, 5762–5766.
5 U. Olsson, K. Shinoda and B. Lindman, *J. Phys. Chem.*, 1986, **90**, 4083–4088.
6 K. Shinoda and H. Saito, *J. Colloid Interface Sci.*, 1968, **26**, 70–74.
7 C. Stubenrauch, *Microemulsions: Background, New Concepts, Applications, Prespectives*, ed. C. Stubenrauch, John Wiley & Sons, Oxford, 2009.
8 L. Magid, P. Butler, K. Payne and R. Strey, *J. Appl. Crystallogr.*, 1988, **21**, 832–834.
9 B. Lindman and U. Olsson, *Ber. Bunsenges. Phys. Chem.*, 1996, **100**, 344–363.
10 R. Strey, *Colloid Polym. Sci.*, 1994, **272**, 1005–1019.
11 K. Shinoda and S. Friberg, *Adv. Colloid Interface Sci.*, 1975, **4**, 281–300.
12 S.-H. Chen, S.-L. Chang and R. Strey, *J. Chem. Phys.*, 1990, **93**, 1907–1918.
13 M. Kotlarchyk, S.-H. Chen, J. S. Huang and M. W. Kim, *Phys. Rev. Lett.*, 1984, **53**, 941–944.
14 K. Fontell, A. Ceglie, B. Lindman and B. Ninham, *Acta Chem. Scand.*, 1986, **40a**, 247–256.
15 W. Jahn and R. Strey, *J. Phys. Chem.*, 1988, **92**, 2294–2301.
16 L. Wolf, H. Hoffmann, K. Watanabe and T. Okamoto, *Phys. Chem. Chem. Phys.*, 2011, **13**, 3248–3256.
17 L. Wolf, H. Hoffmann, Y. Talmon, T. Teshigawara and K. Watanabe, *Soft Matter*, 2010, **6**, 5367–5374.
18 L. Wolf, H. Hoffmann, W. Richter, T. Teshigawara and T. Okamoto, *J. Phys. Chem. B*, 2011, **115**, 11081–11091.
19 L. Wolf, H. Hoffmann, T. Teshigawara, T. Okamoto and Y. Talmon., *J. Phys. Chem. B*, 2012, **116**, 2131–2137.
20 S. Pandey, R. P. Bagwe and D. O. Shah, *J. Colloid Interface Sci.*, 2003, **267**, 160–166.
21 A. Zapf, U. Hornfeck, G. Glatz and H. Hoffmann, *Langmuir*, 2001, **17**, 6113–6118.
22 R. Strey, *Colloid Polym. Sci.*, 1994, **272**, 1005–1019.
23 T. Sottmann and R. Strey, *J. Chem. Phys.*, 1997, **106**, 8606–8615.
24 H. Hoffmann, Plenary lecture, *Prog. Colloid Polym. Sci.*, 1990, **83**, 16–28.
25 R. Aveyard, B. P. Binks, S. Clark and J. Mead, *J. Chem. Soc., Faraday Trans. 1*, 1986, **82**, 125–142.
26 C. Boned, M. Clausse, B. Lagourette, V. E. R. McClean and R. J. Sheppard, *J. Phys. Chem.*, 1980, **84**, 1520–1525.
27 M. J. Kahlweit, *J. Colloid Interface Sci.*, 1987, **118**, 436–453.
28 T. Sottmann, R. Strey and S.-H. Chen, *J. Chem. Phys.*, 1997, **106**, 6483–6491.
29 N. R. Cameron and D. C. Sherrington, *Adv. Polym. Sci.*, 1996, **126**, 162–214.
30 S. Ajith and A. K. Rakshit, *J. Phys. Chem.*, 1995, **99**, 14778–14783.
31 U. Lenz and H. Hoffmann, *Ber. Bunsenges. Phys. Chem.*, 1992, **96**, 809–815.
32 R. Aneyard, B. P. Binks and J. Mead, *J. Chem. Soc., Faraday Trans. 1*, 1985, **81**, 2169–2177.
33 P. Stilbs and B. Lindman, *Prog. Colloid Polym. Sci.*, 1984, **69**, 39–47.
34 O. Söderman and M. Nydén, *Colloids Surf., A*, 1999, **158**, 273–280.
35 S. Gröger, F. Rittig, F. Stallmach, K. Almdal, P. Stepanek and C. M. Papadakis, *J. Chem. Phys.*, 2002, **117**, 396–406.
36 O. Söderman, P. Stilbs and W. S. Price, *Concepts Magn. Reson., Part A*, 2004, **23**, 121–135.

Addition and correction

Note from RSC Publishing

This article was originally published with incorrect page numbers. This is the corrected, final version.

The Royal Society of Chemistry apologises for these errors and any consequent inconvenience to authors and readers.